Indian Journal of Pure & Applied Physics
Vol. 53, June 2015, pp. 409-415

Structure, microstructure and dielectric properties of lead-free BCT-*x*BZT ceramics near the morphotropic phase boundary

Dang Anh Tuan[1,*], VoThanh Tung[1], Truong Van Chuong[1], Nguyen Trong Tinh[2] & Nguyen Thi Mai Huong[2]

College of Sciences, Hue University, Vietnam, Institute of Applied Physics and Scientific Instrument of Vietnamese Academy of Science and Technology, Vietnam

*E-mail:datuan1984gmail.com

Received 16 September 2014; revised 20 January 2015; accepted 25 February 2015

There is an urgent demand for high performance Pb-free piezoelectrics to substitute for the current workhorse, the lead zirconate titanate (PZT) family. In the present study, the high performance lead-free BCT-*x*BZT ceramics near the morphotropic phase boundary (MPB) were prepared by traditional method. The structure, microstructure of the ceramics samples were analyzed. Results show that MPB for these ceramics is achieved with BZT component of $x = 0.48$. Dielectric properties show ferroelectric-relaxor behaviour of this system. Furthermore, the combination of ImageJ and Lince software allows analyzing SEM images of the ceramics for estimating average particle size and particle size distribution.

Keywords: BCT-*x*BZT ceramics, ImageJ, PZT family, Piezoelectrics

1 Introduction

During the past 50 years, Pb-based ceramics such as PZT and modified PZT have exhibited an outstanding piezoelectric performance (d_{33} = 200-600 pC/N, k_{33} = 0.6-0.8). They became promptly main materials in piezodevices[1]. Unfortunately, Pb component in these materials are now facing global restrictions in its usage because of Pb toxicity to the environment and human body. Therefore there is an urgent need to study Pb-free piezoelectric materials with good properties that can compete with PZT family[2,3].

$BaTiO_3$ (BTO) is one of the most basic and widely applied ferroelectric oxide materials with a perovskite-type crystalline structure. It is also dielectric material to fabricate dielectric devices like ceramic capacitors and multilayered ceramic capacitors. It is well known that physical properties of $BaTiO_3$ can be altered by doping with either A or/and B site substitutions[4-6]. For example, the addition of calcium (Ca) into barium (Ba) site and zirconium (Zr) into titanium (Ti) site in barium titanate established compositionally modified BZT and BCT that received much attention due to the tunable structure and the electrical properties to the specific applications[7,8]. What happens when BZT and BCT combine to make new material systems? Wenfeng Liu and Xiaobing Ren[9] designed Pb-free ferroelectric $Ba(Zr_{0.2}Ti_{0.8})O_3$-$x(Ba_{0.7}Ca_{0.3})TiO_3$ systems (BZT-BCT) that have exhibited an equally excellent piezoelectricity as in Pb-based materials[9]. In Liu and Ren's report[9], a very high value of d_{33} is 620 pC/Nwhich can be compared to the PZT material (d_{33} = 500-600 pC/N). They predicted that the single-crystal form of the MPB composition of the Pb-free ferroelectric system may reach enormous d_{33} = 1500-2000 pC/N. The colossal piezo-parameters were received by other researchers for BZT-BCT and modified BZT-BCT materials. For $0.5Ba(Zr_{0.2}Ti_{0.8})O_3$-$0.5(Ba_{0.7}Ca_{0.3})TiO_3$ composition, the values of d_{33} and k_p are 630 pC/N and 0.56, respectively, when the poling conditions were optimized[10]. By modifying 0.06 mol % ZnO in the $Ba_{0.85}Ca_{0.15}Ti_{0.9}Zr_{0.1}O_3$ system, the values[11] of $d_{33}$and k_p are 521 pC/N and 47.8%, respectively. For 0.2 mol. % $BiFeO_3$ doped $Ba_{0.85}Ca_{0.15}Ti_{0.90}Zr_{0.10}O_3$ material[12], the values of d_{33} and k_p possess 405 pC/N and 0.44, respectively. Fairly high d_{33} ~ 423 pC/N and k_p ~ 51.2% values are also obtained for $(Ba_{0.85}Ca_{0.15})(Ti_{0.9}Zr_{0.1})O_3$ compound[13]. Yerang Cui *et al*[14]. found that CeO_2 used as a sintering aid could be enhanced the piezo-parameters for the $(Ba_{0.85}Ca_{0.15})(Ti_{0.9}Zr_{0.1})O_3$ system which owned d_{33} of 600 pC/N and k_p of 0.51. Because of the achieved piezoelectric properties, the BZT-BCT ceramics are suitable for the passive applications such as diagnostic instruments in health, sonar devices in military field, ambient energy harvesting, etc[15-17].

The BCT-BZT systems show a phase diagram with a morphotropic phase boundary (MPB) starting from a triple point of a paraelectric cubic phase (C), ferroelectric rhombohedral (R), and tetragonal (T)

phase that likes Pb contained systems. MPB separates phase diagram into 2 regions with different symmetry: R-phase (BZT side) and T-phase (BCT side). The change of composition ratio *R*/*T* strongly influences the electric properties of the BZT-BCT. The similar results were observed for $Ba(Sn_{0.2}Ti_{0.8})O_3$-$x(Ba_{0.7}Ca_{0.3})TiO_3$ and $Ba(Hf_{0.2}Ti_{0.8})O_3$-$x(Ba_{0.7}Ca_{0.3})TiO_3$ systems[18,19].

In the present work, the lead-free system $(Ba_{0.7}Ca_{0.3})TiO_3$-$xBa(Zr_{0.2}Ti_{0.8})O_3$, or BCT-*x*BZT has been designed, where *x* is a molar per cent of BZT, $x = 0.42 – 0.56$. The effect of BZT concentration on structure and microstructure and some dielectric properties of BCT-*x*BZT system near MPB have also been studied. The optimal properties of these systems around room temperature (just in the MPB temperature regime) are comparable with the MPB composition BCT-48BZT.

2 Experimental Details

A conventional ceramics fabrication technique was used to prepare Pb-free ceramics $(Ba_{0.7}Ca_{0.3})TiO_3$-$xBa(Zr_{0.2}Ti_{0.8})O_3$ ($x = 0.42 – 0.56$) (abbreviated as *x*BZT, with *x* being the molar fraction of BZT). The raw materials with high purity (> 99%) of $BaCO_3$, $CaCO_3$, ZrO_2, TiO_2 were weighed and mixed in a planetary milling machine (PM400/2-MA-Type) using ethanol as a medium for 20 h. The obtained powders were dried in an oven and then calcined at 1250°C for 3 h. After the second milling in ethanol for 20 h, the obtained powders were dried and pressed into disks specimens with a diameter of 12 mm and a thickness of 1.2 mm only by uniaxial pressing with a pressure of 100 MPa. Sintering was carried out at 1450°C for 4 h. The crystalline structure of sintered ceramics was examined by X-ray diffraction (XRD, D8-Advanced, BRUKER AXS). The sintered samples after chemically-etching were cleaned by ultrasonic cleaner. The surface microstructure was observed by scanning electron microscopy (SEM, Nova NanoSEM 450-FEI).The silver pastes were fired at 450°C for 30 min on both sides of these sintered bulks as electrodes for electrical measurements. Dielectric properties of the materials were obtained together using an impedance analyzer (Agilent 4396B, Agilent Technologies, America, HIOKI3532) by measuring the capacitance and phase angle of the specimens from room temperature to 120°C.

3 Results and Discussion

The TGA-DSC curves recorded at a heating rate of 10°C/min in air for an equimolar mixture in stoichiometric proportion of 0.48BZT composition is shown in Fig. 1. There are two distinct weight losses in the TG curve corresponding to two endothermic peaks in the TGA curve. The first weight loss occurs around 709°C, and the second one locates at 927°C with weight losses in percentage of 6.974 and 17.643, respectively. In principle, a solid reaction occurs completely to form BZT-BCT solid solution at the second endothermic peak (corresponding to the highest weight loss in the investigated temperature region). It means that the temperature for calcination was chosen around 927°C. However, the initial mass of mixture in stoichiometric proportion was used for measuringTGA-DSC curves, was very small as compared to the amount of the raw materials in our work, thus calcining temperature was selected over 250-300°C than endothermic peak, i.e. 1200-1250°C. These temperatures were also selected by other researchers[20-23].

Figure 2(a) shows the XRD patterns of *x*BZT ceramics, measured at room temperature. All ceramics exhibit a pure perovskite phase and no secondary phase was observed in the range investigated. The stable solid solutions were well established. Figure 2(b) shows the expanded XRD patterns in the range 44°-46° of *x*BZT ceramics. The BZT contents of 0.42-0.44, *x*BZT ceramics have tetragonal symmetry characterized by splitting (002)/(200) peaks at around 2Theta of 45°. The intensity of $(002)_T$ peak decreases with increasing BZT content. The (200) and (002) diffraction peaks of *x*BZT ceramics gradually merge with the BZT content beyond 0.48, confirming an involvement of a phase transition. More clearly, we fitted XRD data of the

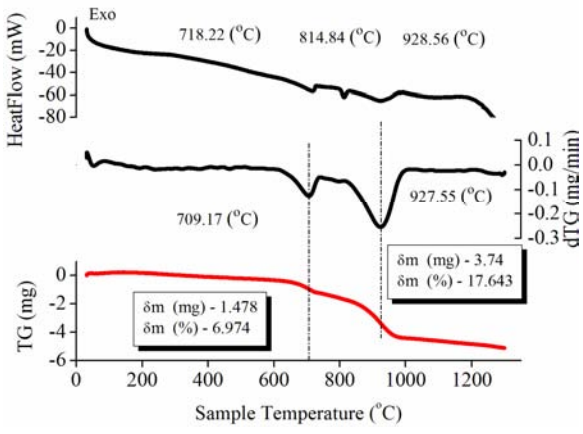

Fig. 1 — TGA-DSC curves for the mixture in stoichiometric proportion of 0.48BZT

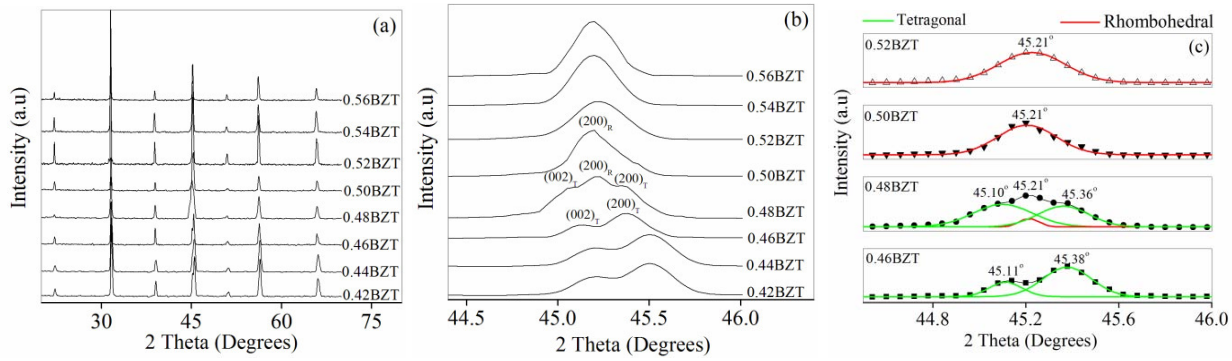

Fig. 2 — XRD partten of *x*BZT ceramics

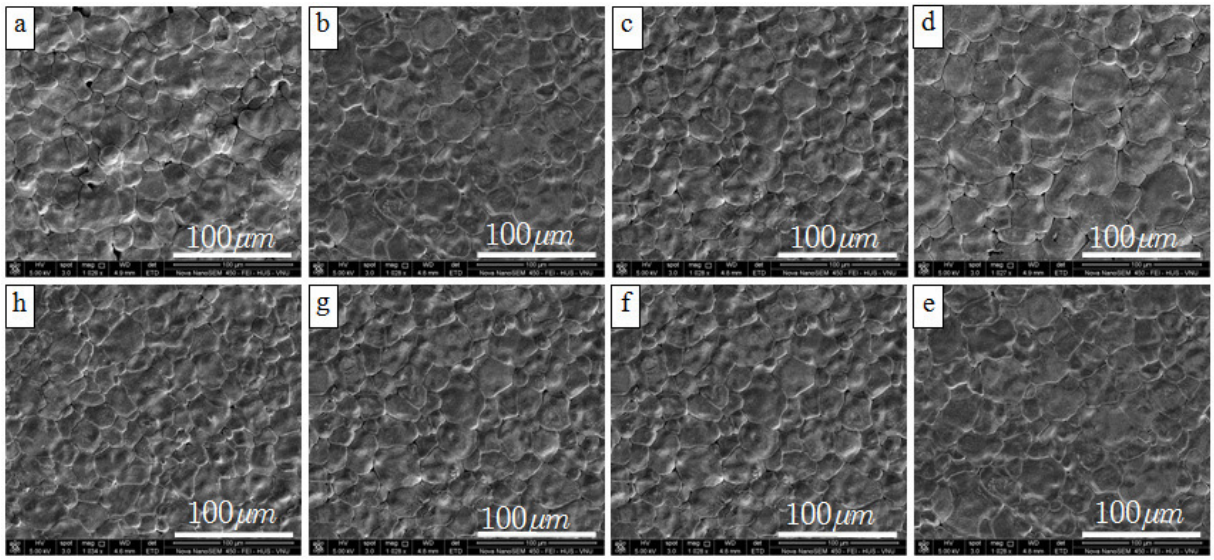

Fig. 3 — Surface morphologies of *x*BZT ceramics: (a) 0.42BZT, (b) 0.44BZT, (c) 0.46BZT (d) 0.48BZT, (e) 0.50BZT, (f) 0.52BZT, (g) 0.54BZT, (h) 0.56BZT

samples around 0.48BZT composition with Gauss function [Fig. 2(c)]. As shown in Fig. 2(c), the sample 0.48BZT contains two phases simultaneously: tetragonal phase [$(002)_T$, $(200)_T$ peaks positioned at 45.11°, 45.36°, respectively] and rhombohedral phase ($(200)_R$ located at 45.21°). Moreover, the diffraction peak positions shift to the lower angles as increasing BZT content. The BZT concentration can lead to crystal lattice distortion and change in crystalline structure. On the other hand, the coexistence of tetragonal-rhombohedral phases was observed at $x = 0.48$, implying that MPB is located at 0.48BZT composition. This result is different from previous report[9], where MPB composition is $x = 0.50$.

Figure 3 shows the surface morphologies of the polished and chemically-etched *x*BZT ceramics. No secondary phase or phase segregation at grain boundary was detected. In order to estimate grain size, the microstructural photos of the ceramics were analyzed using ImageJ software[24,25]. Figure 4 shows the particle size distribution with data obtained from ImageJ software. The grain sizes are located between 5 and 95 μm and gathered round the top of Gauss fitting plot. As a comparison, a linear cutting method using Lince software[26] was performed to determine average grain size (Table 1).

Figure 5(a) shows the BZT concentration dependence of permittivity and dielectric loss of the *x*BZT ceramics at 1 kHz and room temperature. It can be seen that BZT content has strong effect on dielectric properties. As amount of BZT increases, the values of permittivity and dielectric loss vary simultaneously and reach the maximum of 3321 and the minimum of 1.3% at 0.48BZT composition,

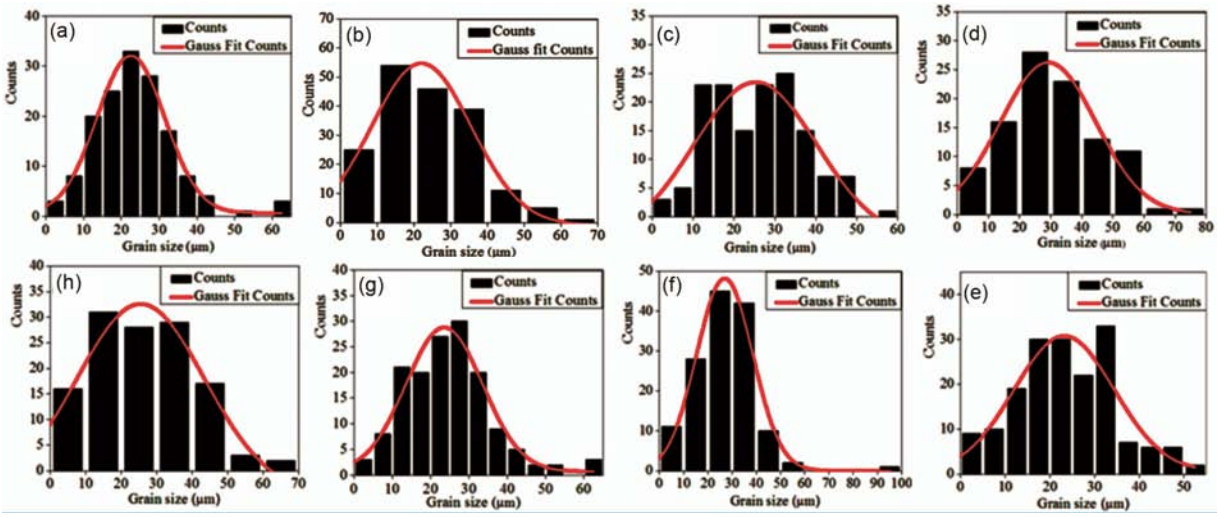

Fig. 4 — Grain size distribution for *x*BZT ceramics: (a) 0.42BZT, (b) 0.44BZT, (c) 0.46BZT (d) 0.48BZT, (e) 0.50BZT, (f) 0.52BZT, (g) 0.54BZT, (h) 0.56BZT

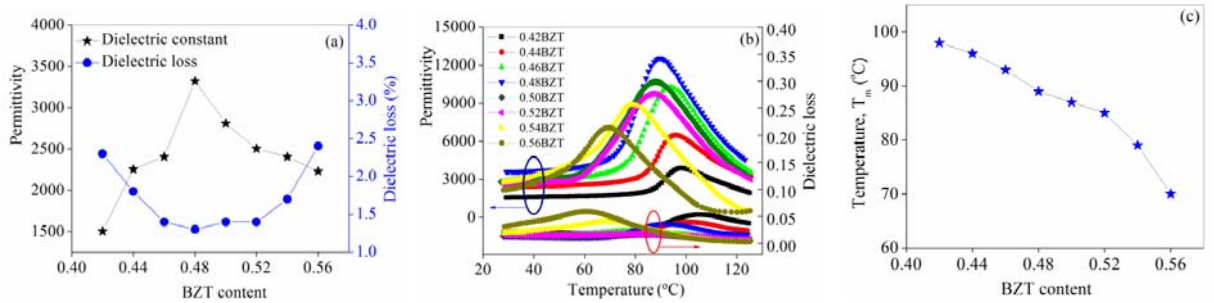

Fig. 5 — (a) Permittivity and dielectric loss as a function of BZT content at 1 kHz, room temperature, (b) The plot of T_m versus BZT content, and (c) Temperature dependence of permittivity and dielectric loss of *x*BZT ceramics

Table 1 — Grain size for *x*BZT ceramics

BZT content,*x*	Grain size (μm)		Density (kg/m^3)
	Lince software	Image J software	
0.42	22.6	22.5	5351
0.44	24.1	22.0	5482
0.46	28.4	25.2	5534
0.48	32.4	29.2	5624
0.50	30.0	25.5	5602
0.52	26.4	23.5	5531
0.54	27.9	27.0	5493
0.56	24.8	23.2	5452

respectively. This result could be due to the variation in grain size of the (Ba, Ca)(Zr, Ti)O_3 ceramics[27].

Measurements on the dielectric permittivity as a function of the temperature reveal anisotropic behaviour. The highest permittivity of 12514 is observed for the 0.48BZT composition (as shown in Fig. 6). The temperature, T_m, corresponding to the maximum permittivity, ε_m, reduces with the increase of BZT concentration due to the change in crystal structure as shown in XRD pattern. The top of permittivity-temperature curves is broadened, indicating of a ferroelectric relaxor behaviour in the literature[28-30].

A modified empirical expression was proposed by Uchino and Nomura[31] to describe the diffuseness of the ferroelectric phase transition as:

$$\frac{1}{\varepsilon}-\frac{1}{\varepsilon_m}=\frac{(T-T_m)^{\gamma}}{C},\quad (1\le\gamma\le 2) \qquad \ldots(1)$$

\where γ and C are assumed to be constant. The parameter γ, called degree of diffuseness, gives information on the character of phase transition. As γ = 1, expression given in Eq. (1) describes a normal Curie-Weiss law and γ = 1 that presents a complete diffuse phase transition. The plots of $\ln(1/\varepsilon - 1/\varepsilon_m)$

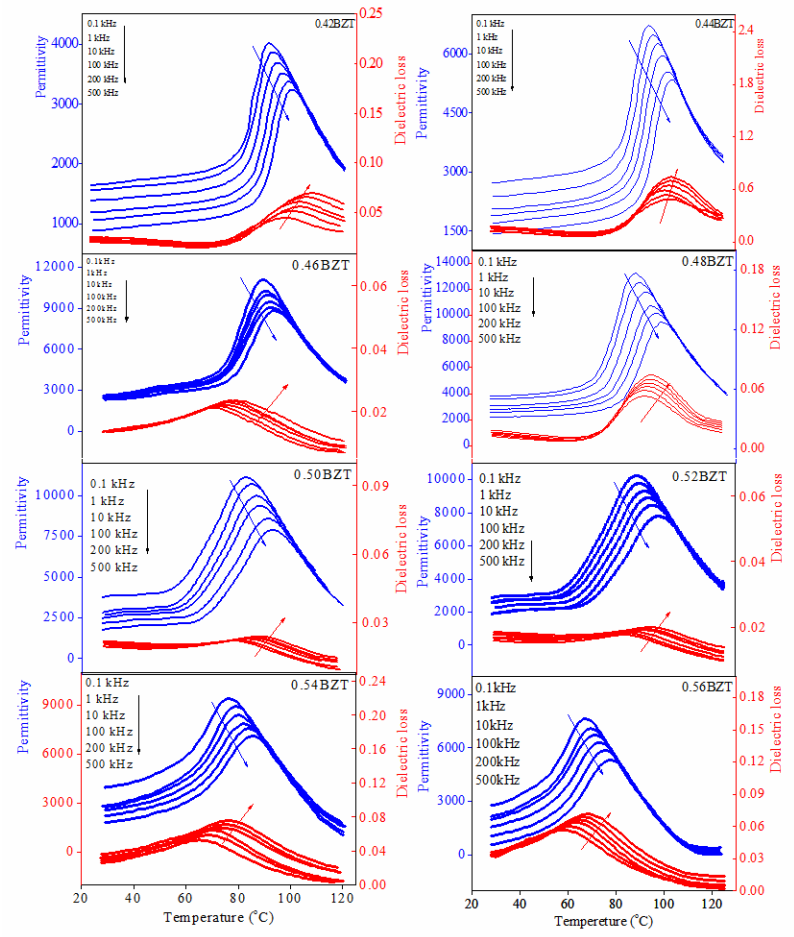

Fig. 6 — Temperature dependence of permittivity and dielectric loss of *x*BZT ceramics at various frequencies

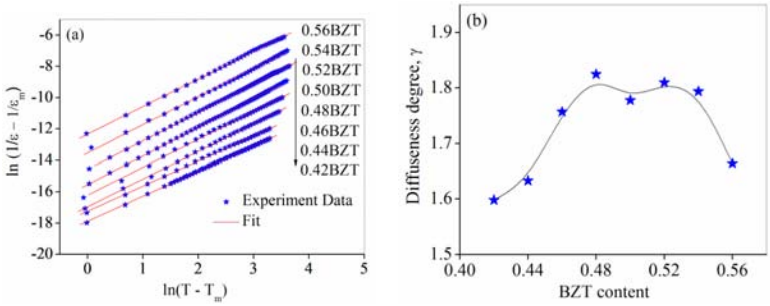

Fig. 7 — (a) $\ln(1/\varepsilon - 1/\varepsilon_m)$ as a function of $\ln(T - T_m)$ at 1 kHz for the *x*BZT ceramics, (b) BZT content dependence of diffuseness degree, γ

versus $\ln(T - T_m)$ of *x*BZT ceramics at 1 kHz are shown in Fig. 7(a). The parameter γ varies as increasing BZT and reaches the highest value of 1.825 at 0.48 BZT composition. It is said that the transitions are of diffuse type, and the ceramics are highly disordered. By fitting Eq. (1) to the data, the γ constant is obtained from the s loop of the fitting curves. Figure 7(b) shows the dependence of γ versus BZT concentration.

To study the frequency dependence of T_m, it is necessary to apply Vogel-Fulcher relationship[32,33]

$$f = f_o \exp\left[-\frac{T_o}{T_m - T_f}\right] \qquad \ldots(2)$$

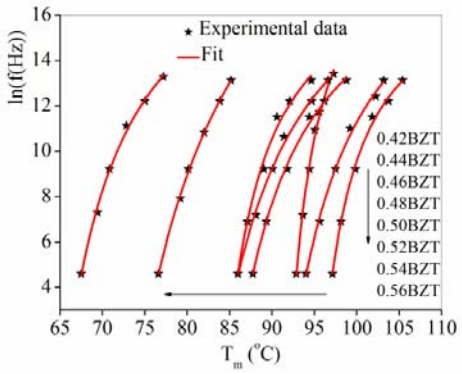

Fig. 8 — Plot of ln(f) versus T_m for the xBZT ceramics. The symbols are the experimental points, and the fitted lines correspond to Vogel-Fulcher law

Table 2 — Values of T_o , T_f (°C), with various BZT content, x

x	0.42	0.44	0.46	0.48	0.50	0.52	0.54	0.56
T_o	68	157	66	150	191	87	340	147
T_f	92	85	89	78	75	80	62	59

where, is the attempt frequency, and is a constant. The parameters T_o, T_f, were obtained by fitting experiment data in Eq. (2) and listed in Table 2. A good fit of the data with Vogel-Fulcher equation (Fig. 8) confirms a static freezing temperature of thermally activated polarization fluctuations in xBZT ceramics.

4 Conclusions

Complete perovskite lead-free xBZT ceramics were prepared by using the solid state reaction method. As varying BZT content, the structure of the material changes from tetragonal phase to rhombohedral phase. At 0.48BZT composition, the tetragonal and rhombohedral phases coexist which demonstrates that MPB is located at this composition. Our work indicates that with x = 0.48, the characteristic parameters such as density, dielectric constant, average grain size reach maximum values[3], which are 5624 kg/m12514, 32.4 µm, respectively. The results also show the diffuse transitions in the material. The experimental T_m data points are found to be in good agreement with Vogel-Fulcher relationship which constitutes strong evidence for a static freezing temperature of thermally activated polarization fluctuations in lead-free ceramics BZT-BCT.

Acknowledgement

The work was carried out in the frame of the "Basic Project of Hue University 2013-2015".

References

1 Haertling G H, *J Am Ceram Soc*, 82 (1999) 797.
2 Shrout T R & Zhang S J, *J Electroceram*, 19 (2007) 113.
3 Takenaka T & Nagata H, *J Eur Ceram Soc*, 25 (2005) 2693.
4 Thakur O P, Prakash C & James A R, *J Alloys Compd*, 470 (2009) 548.
5 Wang X S, Yamada H & Xu C N, *Appl Phys Lett*, 86 (2005) 022905.
6 Halder S, Gerber P, Schneller T & Waser R, *Appl Phys A*, 81 (2005) 11.
7 Maiti T, Guo R & Bhalla A S, *Appl Phys Lett*, 89 (2006) 122909.
8 Varatharajana R, Samantab S B, Jayavela R, Subramanian C, Narlikar A V & Ramasamy P, *Materials Characterization*, 45 (2000) 89.
9 Liu Wenfeng & Ren Xiaobing, *Physical Review lett*, 103 (2009).
10 Su Shi, Zuo Ruzhong, Lu Shengbo, Xu Zhengkui, Wang Xiaohui & Li Longtu, *Curr Appl Phys*, 11 (2011) 120.
11 Wu Jiagang, Xiao Dingquan, Wu Wenjun, Chen Qiang, Zhu Jianguo, Yang Zhengchun & Wang John, *Scripta Materialia*, 65 (2011) 771.
12 Wu Jiagang, Wu Wenjuan, Xiao Dingquan, Wang John, Yang Zhenchun, Peng Zhihang, Chen Qiang & Zhu Jianguo, *Curr Appl Phys*, 12 (2012) 534.
13 Wu Jiagang, Xiao Dingquan, Wu Wenjuan, Chen Qiang, Zhu Jianguo & Yang Zhengchun, *J of the European Ceramic Society*, 32 (2012) 891.
14 Cui Yerang, Liu Xinyu, Jiang Minhong, Zhao Xiayan, Shan Xu, Li Wenhua, Yuan Changlai & Zhou Changrong, *Ceramics Inter*, 38 (2012) 4761.
15 Choi K, Keilers C H Jr & Chang F K, *Structural Dynamics & Materials Conf*, 1 (1994) 118.
16 Qi Tingting, Grinberg Ilya, Bennett Joseph W, Shin Young-Han, Rappe Andrew M, Yeh Ka-Lo & Keith A Nelson, *DoD High Performance Computing Modernization Program Users Group Conference* (2010).
17 Wu Weiwei, Cheng Li, Bai Suo, Dou Wei, Xu Qi, Wei Zhiyang & Qin Yong, *J of Materials Chemistry A*, 25 (2013).
18 Xue Dezhen, Zhou Yumei, Bao Huixin, Gao Jinghui & Zhou Chao, *Appl Phys Lett*, 99 (2011) 122901.
19 Zhou Chao, Liu Wenfeng, Xue Dezhen, Ren Xiaobing & Bao Huixin, *Appl Phys Lett*, 100 (2012) 222910.
20 Cui Yerang, Liu Xinyu, Jiang Minhong, Hu Yaobin, Su Qingshuang & Wang Hua, *J Mater Sci* Mater Electron, 23 (2012) 1342.
21 Li Wei, Xu Zhijun, Chu Ruiqing, Fu Peng & Zang Guozhong, *J Am Ceram Soc,* 93 (2010) 2942.
22 Wu Jiagang, Xiao Dingquan, Wu Wenjun, Chen Qiang, Zhu Jianguo, Yang Zhengchun & Wang John, *Scripta Materialia*, 65 (2011) 771.
23 Hao Jigong, Bai Wangfeng, Li Wei & Zhai Jiwei, *J Am Ceram Soc*, 1-9 (2012).
24 Schneider CA, Rasband W S & Eliceiri K W, *Nature Methods*, 9 (2012) 671.
25 Abramoff M D, Magalhaes P J & Ram S J, *Biophotonics Inter*, 11 (2004) 36.

26 http://wwwmawitu-darmstadtde/naw/nawstartseite/kompetenzen/gefuegeeigenschaften/sv_softwareenjsp
27 Tang Xin-Gui, *J of Appl* Phys, 97 (2005) 034109.
28 Wada S, Suzuki S, Noma T, Kakihana M, Park S E, Cross L E & Shrout T R, *Jpn J Appl Phys,* 38 (1999) 5505.
29 Park S E, Wada S, Cross L E & Shrout T R, *J Appl Phys*, 86 (1999) 2746.
30 Ravez J & Simon A, *Eur J Solid State Inorg Chem*, 34 (1997) 1199.
31 Uchino K & Nomura S, *Integr Ferroelectr* 44, (1982) 55.
32 Samara G A, Venturini E L, *Phase Transitions,* 79 (2006) 21.
33 Pirc R & Blinc R, *Phy Rev B,* 76 (2007) 1.